Viscoelastic Characterization of Electrochemically Prepared Conducting Polymer Films by Impedance Analysis at Quartz Crystal

Study of the Surface Roughness Effect on the Effective Values of the Viscoelastic Properties of the Coating

A. Arnau,[a,z] Y. Jimenez,[a] R. Fernández,[a] R. Torres,[a] M. Otero,[b] and E. J. Calvo[c,*]

[a]*Departamento Ingeniería Electrónica, Universidad Politécnica de Valencia, Camino de Vera s/n, 46022 Valencia, Spain*
[b]*Departamento de Física/CONICET, and [c]INQUIMAE, Departamento de Química Inorgánica Analítica y Química Física, Facultad de Ciencias Exactas y Naturales, Universidad de Buenos Aires, Pabellón 2, Ciudad Universitaria, AR-1428 Buenos Aires, Argentina*

An electrochemical quartz crystal microbalance is used for a continuous monitoring of the growth of the polymer poly(3,4-ethylenedioxy) thiophene tetrabutylammonium perchlorate (PEDOT-TBAP), electropolymerized in acetonitrile on a gold electrode of a 10 MHz AT-cut quartz crystal resonator. The surface acoustic impedance of the resonator is analyzed starting from the electrical admittance continuously measured by means of a network analyzer. Changes in the acoustic impedance suggest that a mechanical resonance phenomenon occurs during the electrodeposition. To determine the origin of this effect, the evolution of the physical properties of the coating is analyzed. This analysis shows a significant change of the viscoelastic properties of the coating during the electropolymerization and especially during the time interval of the suspected mechanical resonance. The effect of the surface roughness on the mechanical impedance of the coating is analyzed. This study seems to indicate that the changes in the effective viscoelastic properties of the coating are due to the changes in the surface roughness. The mechanical resonance effect also seems to be more a result of this change in the coating effective viscoelastic properties than of the growth of the coating thickness where coating viscoelastic properties are maintained constant.
© 2006 The Electrochemical Society. [DOI: 10.1149/1.2195893] All rights reserved.

Polythiophenes are high conductive polymers with high chemical and thermal stability. Due to their high electrical conductivity, polythiophenes find interesting uses in different applications, such as patterned circuits (plastic circuits), photodiodes,[1] biosensors,[2] antistatic coatings,[3] corrosion protection coatings,[4] etc. However, they have not been extensively used due to the changes of their properties, which have been observed over the course of time when coming in contact with the environment. Moreover, relatively little is known about the mechanical properties, such as shear moduli, of these polymer layers, whose thicknesses can range from some nanometers to micrometers depending on applications.

The quartz crystal resonator (QCR) technique can be useful for estimating these properties and their change during the polymer growth. Furthermore, other effects regarding the macroscopic structure of the polymeric coating can contribute to the sensor response and be analyzed, in particular the roughness effect, intimately related to the porosity and with the hydration grade.

Some results in this field were reported by Hillman and co-workers, who described the viscoelastic effects of polythiophenes by means of an electrochemical quartz crystal microbalance (EQCM),[5-7] including the evolution from gravimetric to viscoelastic response in poly(3-methylthiophene) films[8] and the acoustic phenomenon of film resonance in poly(3-methylthiophene) in contact with liquid electrolyte.[9] The reports of "film resonance" in quartz crystal resonators are almost entirely focused on thiophenes. It has been our interest to report film resonances with poly(3,4-ethylenedioxy thiophene) (PEDOT) and most importantly to show that the effect is strongly affected by the surface roughness and morphology. The latter has been neglected in previous studies of film resonances in conducting polymers and poses important questions about the interpretation in the reported cases.

Ivasta and co-workers reported the electrochemical polymerization of 3,4-ethylenedioxithiophene (EDOT) in different electrolyte-solvent media with the EQCM.[10]

Recently, it has been shown that the electrochemical polymerization of electrically conducting polymers such as thiophenes on the gold electrode of an EQCM produces porous and fibrous surfaces whose degree of porosity depends on the polymer, on the technique used for the electropolymerization, the speed of the polymer growth, etc.[11,12] Topart and co-workers studied the morphological changes induced by ion movement in electropolymerized EDOT films by using EQCM.[13] Bund and co-workers, by including roughness models in their studies with conductive polymers on EQCM, have shown that the morphology of the surface roughness modifies as the polymer grows.[12,14]

It should be clearly indicated that the response of a coated resonant sensor is not free from the coating surface roughness contribution when a viscous semi-infinite medium (electrolyte) is on top. The electrolyte penetrates in the pores and cavities of the polymer and additional inertial and loss effects appear, whose contribution on the sensor response depends on different parameters of the roughness, such as the characteristic height of the roughness, the surface of the roughness, and the volume of liquid displaced by the volume of the roughness in its oscillatory movement.[15,16]

In general, the studies on conductive polymers carried out through an EQCM do not include models accounting for the contribution of the polymer roughness on the sensor response. Thus, the EQCM layer-model used corresponds to the three-layer model shown in Fig. 1a, where the polymer layer, the so-called coating, is assumed to have an effective uniform thickness $h_{1|ef}$, with effective viscoelastic properties $G'_{1|ef}$ and $G''_{1|ef}$, storage, and loss shear moduli, respectively. Therefore, the three-layer model is used to represent a situation which can be modeled in a more real way as shown in Fig. 1b, where a rough layer is included in a four-layer model where the coating layer is divided in two: one uniform layer at the bottom with uniform thickness h_1 and viscoelastic properties G'_1 and G''_1 and a rough layer on top with characteristic parameters of the roughness ξ (magnitude relative to the porosity) and L_r (thickness of the rough layer). Then, the physical properties of the polymer layer extracted when considering the three-layer model should be considered as effective properties which include additional effects such as roughness.
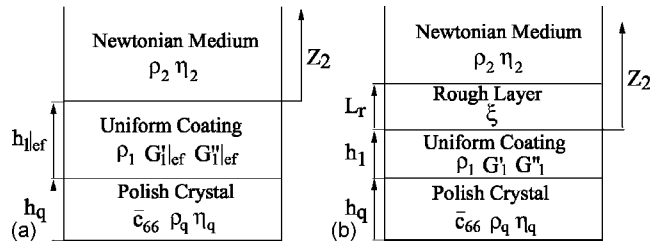
Figure 1. Cross sections of different models of a coated TSM resonator: (a) Three-layer model: quartz + uniform coating layer + liquid, and (b) four-layer model: quartz + uniform coating layer + rough layer + liquid.

In the present article, we report studies of the electrochemical growth of PEDOT in acetonitrile with tetrabutylammonium with an EQCM. The analysis of the surface acoustic load impedance during the polymer growth shows the evolution from gravimetric to viscoelastic regimes, a response that suggests a film mechanical resonance is also observed. The evolution of the effective properties of the polymer layer following the three-layer model shown in Fig. 1a was analyzed and a significant change in the effective viscoelastic properties was observed. The contribution of the surface roughness on the acoustic load impedance response was also analyzed: for the gravimetric acoustic regime, through a new roughness model recently introduced by the authors, which is outlined below, and for the viscoelastic acoustic regime by means of a new algorithm recently developed by the authors. This study seems to indicate that changes in the surface roughness, probably due to a compacting process of the polymer layer during the electrodeposition, are responsible for the changes in the effective viscoelastic properties of the coating. The mechanical resonance effect also seems to be more the result of this change in the coating effective viscoelastic properties than the result of a growth of the coating thickness where the viscoelastic properties of the coating are maintained constant.

The admittance model and the problem of parameter extraction.— The most comprehensive one-dimensional model for representing the response of a coated quartz crystal resonator (QCR) is given by the transmission line model (TLM), which provides the electrical admittance of the sensor as follows[17,18]

$$Y = G + jB = j\omega C_0^* + \frac{1}{Z_m} \quad [1]$$

where $C_0^* = C_0 + C_{ex}$, C_0 being the so-called static capacitance, and C_{ex} an added external parallel capacitance accounting for packaging, connection, etc. Z_m is the impedance of the so-called motional branch, which can be expressed as the additive contribution of the motional impedance of the sensor in the unperturbed state, Z_m^0, and a term associated with the load, Z_m^L, as follows

$$Z_m = \frac{1}{j\omega C_0}\left(\frac{\frac{\alpha_q}{K^2}}{2\tan\frac{\alpha_q}{2}} - 1\right) + \frac{1}{\omega C_0}\frac{\alpha_q}{4K^2}\frac{Z_L}{Z_{cq}}\frac{1}{1 - \frac{j\frac{Z_L}{Z_{cq}}}{2\tan\alpha_q/2}}$$

$$= Z_m^0 + Z_m^L \quad [2]$$

where K is the complex electromechanical coupling factor for a lossy quartz, α_q is the complex acoustic wave phase across the lossy quartz, Z_{cq} is the quartz characteristic impedance, and Z_L is the acoustic load impedance. The parameters C_0, K, α_q, and Z_{cq} in Eq. 2 depend on intrinsic properties of quartz (Table I) and on the crystal thickness h_q, the electrode area A_s, and the quartz crystal losses η_q in the following way

$$C_0 = \varepsilon_{22}\frac{A_s}{h_q}, \quad K = \sqrt{\frac{e_{26}^2}{\varepsilon_{22}\bar{c}_{66}}}, \quad \alpha_q = h_q\omega\sqrt{\frac{\rho_q}{\bar{\bar{c}}_{66}}},$$

Table I. Properties of a 10 MHz AT-cut quartz crystal.

Quartz parameter	Value	Description
ε_{22}	3.982×10^{-11} A^2 s^4 kg^{-1} m^{-3}	Permittivity
η_q	9.27×10^{-3} Pa s	Effective viscosity
$\bar{c}_{66}$	2.947×10^{10} N m^{-2}	Piezoelectrically stiffened shear modulus
e_{26}	9.657×10^{-2} A s m^{-2}	Piezoelectric constant
ρ^q	2651 Kg m^{-3}	Density
A_S	2.92×10^{-5} m^2	Effective electrode surface area
h_q	166.18×10^{-6} m	Thickness

$$Z_{cq} = \sqrt{\rho_q\bar{\bar{c}}_{66}} \quad \bar{\bar{c}}_{66} = \bar{c}_{66} + j\omega\eta_q \quad [3]$$

The effective values of the crystal thickness h_q^{ef}, the static capacitance C_o^{ef}, the quartz crystal losses η_q^{ef}, and the external parallel capacitance C_{ex} must be obtained by sensor calibration. The physical and geometrical properties of the layers deposited on the crystal are included in the acoustic load impedance Z_L

$$Z_L = Z_1^c\frac{Z_2 + Z_1^c\tanh(\gamma_1 h_1)}{Z_1^c + Z_2\tanh(\gamma_1 h_1)} \quad [4]$$

where $Z_1^c = (\rho_1 G_1)^{1/2}$ is the characteristic impedance of the coating, $G_1 = G_1' + jG_1''$ being the complex shear modulus, and ρ_1 the density; $\gamma_1 = j\omega\rho_1/Z_1^c$ is the complex wave propagation factor in the coating, h_1 is the coating thickness, and Z_2 is the acoustic load impedance at the coating surface. Z_2 corresponds, in the three-layer model shown in Fig. 1a, to the characteristic impedance of the semi-infinite medium, where $Z_2 = (\rho_2 G_2)^{1/2}$ with ρ_2 and G_2 the density and the complex shear modulus of the second medium, respectively, and Z_2 corresponds, in the four-layer model depicted in Fig. 1b, to the terminal acoustic impedance seen from the coating interface which represents the contribution of the rough layer in contact with the liquid. Some models for Z_2 can be found elsewhere.[11,14-16,19]

When Z_L is small compared to the mechanical impedance of the quartz crystal itself Z_{cq} (8.849×10^6 kg m^{-2} s^{-1} for an AT-cut quartz crystal), the so-called "small surface load impedance condition" occurs and the acoustic load approximation (Eq. 5) can be applied directly from Eq. 2.[20]

$$Z_L = Z_{cq}\frac{4K^2\omega C_o}{\pi}\Delta Z_m \quad [5]$$

where $\Delta Z_m = Z_m - Z_m^0 = Z_m^L$ is the electrical motional impedance shift taken as the difference between the coated and uncoated device.

Unchanged quartz parameters allow for a direct relation between the complex acoustic impedance, Z_L, and two directly measurable values: the motional series resonant frequency shift, Δf_s, at the in-phase admittance value, which is normally taken as the frequency shift between the maximum conductance values at resonance for the coated and uncoated device, and the change in the motional resistance, ΔR_m, taken as the difference in the reciprocal of maximum conductance magnitudes between the coated and uncoated device, as follows[18,20]

$$R_L = Z_{cq} \frac{4K^2 \omega C_o}{\pi} \Delta R_m \qquad [6]$$

$$X_L = - \frac{\pi Z_{cq}}{f_o} \Delta f_s \qquad [7]$$

When $Z_2 \ll Z_1^c$, the acoustic load impedance in Eq. 4 results in the additive contribution of the acoustic impedances of the coating and the liquid as follows

$$Z_L = Z_2 + Z_1^c \tanh(\gamma_1 h_1) \qquad [8]$$

For thin ($h_1 \to 0$), rigid ($G_1'' = 0$) layers, the former equation reduces to $Z_L = Z_2 + j\omega\rho_1 h_1$, which applied on Eq. 6 and 7 reproduce the well-known Martin's model[21] (Eq. 9) which claims direct additive contributions of the liquid (Kanazawa relation[22]) and surface mass density of the coating $m_s = \rho_1 h_1$ (Sauerbrey relation[23]) on the frequency shift, while the motional resistance shift is only associated with the damping due to the liquid

$$\Delta f_s|_{\text{liquid+coating}} = \Delta f_s|_{\text{liquid}} + \Delta f_s|_{\text{coating}}$$

$$= - \frac{f_o}{\pi Z_{cq}} \sqrt{\frac{\rho_2 \eta_2 \omega}{2}} - C_{SB}\rho_1 h_1 \qquad [9]$$

For a 10 MHz AT-cut quartz crystal, the Sauerbrey constant is

$$C_{SB} = 2f_o^2/Z_{cq} = 226.01 \text{ Hz cm}^2 \text{ } \mu g^{-1}$$

In the context of Fig. 1a, when no approximation can be done about the layer, i.e., when it is not reasonable to consider a Sauerbrey-like behavior of the coating, or the "small surface load impedance condition" cannot be applied, the appropriate admittance model for characterizing the electrical response of the sensor turns into the TLM in Eq. 1, and the coating properties have to be extracted starting from electrical measurements. For the three-layer compound represented in Fig. 1a, and assuming the mentioned crystal parameters, h_q, A_q, η_q, and C_{ex}, to be known or obtained by calibration, there are seven unknowns, four of them correspond to the coating (h_1, ρ_1, G_1', G_1'') and the other three to the semi-infinite medium (ρ_2, G_2', G_2''). These unknowns can be reduced to four: h_1, ρ_1, G_1', G_1'' when the properties of the second medium are known. Furthermore, the acoustic load impedance Z_L can be written as a function of only three parameters of the coating with physical significance, for instance the magnitude of the characteristic acoustic impedance, $|Z_1^c| = (\rho_1|G_1|)^{1/2}$, the quality factor, $Q_1 = 1/\tan\delta_1 = G_1'/G_1''$, and the surface mass density, $m_s = \rho_1 h_1$, as indicated in Eq. 10 and 11

$$Z_1^c = \sqrt{\rho_1 G_1} = \sqrt{\rho_1 |G_1|} e^{j(\delta_1/2)} = |Z_1^c| e^{j(\delta_1/2)} \qquad [10]$$

$$\gamma_1 h_1 = j\omega \sqrt{\frac{\rho_1}{G_1}} h_1 = j\frac{\omega m_s}{|Z_1^c|} e^{-j(\delta_1/2)} \qquad [11]$$

This is of fundamental importance because it indicates that the problem of the four parameters extraction, h_1, ρ_1, G_1', G_1'', is inherently undetermined starting only from the global admittance spectrum, because any combination of these four parameters which provide the same values for $|Z_1^c|$, Q_1, and m_s will provide the same admittance response in all the frequency spectrum. Thus, a complete extraction of the four properties requires at least the knowledge of one of them, for instance the density, which has to be obtained from literature or obtained by means of an alternative technique. Therefore, the problem of uniqueness in the extraction of the coating properties, starting only from electrical measurements, can only be coherently formulated if the objective is the obtaining of the corresponding triad of properties $|Z_1^c|$, Q_1, and m_s. Because they are three unknowns, the problem is clearly undetermined for those systems, typically based on oscillators, which only provide two experimental data; infinite possible solutions provide the same couples of experimental data and it is impossible to make, with the exception of limiting cases, any coherent interpretation. For those systems that provide more

than two experimental data (impedance and network analyzers), the problem of parameter extraction can be, in principle, determined; however, its solution is one of the challenging tasks of QCR applications, not completely solved even in theoretical conditions. An overview of the strategies used by different authors to face the problem can be found elsewhere.[18,24,26]

Recently, the authors have developed an algorithm that permits an unambiguous extraction of the three properties of the coating (m_s, Q_1, and $|Z_1^c|$) under theoretical conditions, starting only from the admittance spectrum of the sensor around resonance.[24,26]

Basically the algorithm contains four steps. The first and second steps are preliminary steps used for calibration; the third step provides a set of triads of coating properties (m_s, Q_1, and $|Z_1^c|$) which are solutions of the problem at one frequency of the admittance spectrum, normally selected near the maximum conductance frequency (ω_1). As only one experimental frequency is selected, an infinite number of curves (triads) are theoretically possible to coincide at that frequency, only restricted by the physical range of properties established and the necessary discretization of the properties to make the calculation accessible. In the fourth step, the optimum triad is selected. In theoretical conditions the selection of the optimum triad is made through a fitting algorithm of the TLM to the experimental admittance data. However, from a practical point of view, when the experimental plot and the one derived from the TLM for the optimum triad do not have an excellent matching, it is necessary to introduce an additional restriction in order to reduce the propagation error in the selection of the set of triads obtained in the third step. In this case, the algorithm enables us to perform an error analysis of the extracted properties as a function of the estimated error for the value of the magnitude obtained with the alternative technique. For EQCM applications, the additional restriction could be the coating surface mass density, whose theoretical magnitude can be estimated during the electrochemical process through the charge measurement when the efficiency is assumed to be known.

Apart from the improvements in relation to other routines, the algorithm can distinguish the solutions which correspond to different resonances and then use this information to restrict the solution in a coherent way. Moreover, the algorithm also provides a powerful tool that enables us to analyze the contribution of certain phenomena not considered by the TLM, such as roughness or slip, on the effective properties of the coating. This application is very useful for the interpretation of the experimental results; therefore, this utility is developed later on in the discussion of the experimental part. A more detailed description of the algorithm can be found elsewhere.[24-26]

Impedance contribution of a rough layer.— The influence of roughness on the resonance behavior of a quartz crystal has been discussed by Schumacher,[27] Martin et al.,[28] Urbakh and Daikhin,[19,29] and Etchenique.[11] The most complete current models for describing the mechanical acoustic impedance of a rough surface with a liquid on top, Z_2 as shown in Fig. 1b, are the Urbakh and Daikhin, and Etchenique models. These are two-parameter models, the thickness of the layer L_r and its lateral dimension ξ (characteristic length of porosity[11]), which are also valid for large surface roughness. The term large has to be seen in relation to the viscous penetration depth in the liquid given by $\delta_2 = \sqrt{\eta_2/(\pi f \rho_2)}$ where η_2 is the viscosity of the liquid and ρ_2 its density. The characteristic impedance Z_2 as described in Fig. 1b for these models is[11,14,24]

$$Z_2 = j\omega\rho_2 \left[\frac{1}{K_0} + \frac{L_r}{\xi^2 K_1^2} - \frac{1}{M\xi^2 K_1^2} \left(\frac{2K_0}{K_1}[\cosh(K_1 L_r) - 1] \right. \right.$$

$$\left. \left. + \sinh(K_1 L_r) \right) \right] \qquad [12]$$
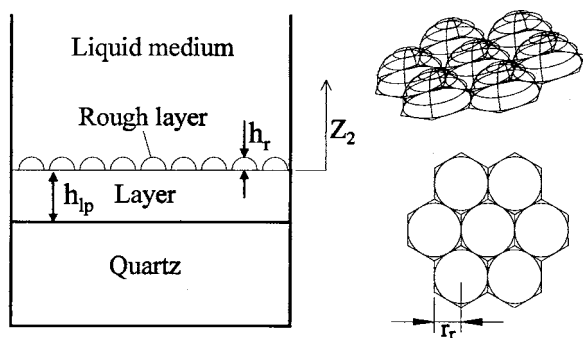
Figure 2. Model for surface roughness based on a rough surface covered by spherical shells of characteristic dimensions h_r (height of the shell) and r_r (radius of the circular base of the shell).

for the Daikhin and Urbakh model, and

$$Z_2 = j\omega\rho_2\left[\frac{1}{K_0} + \frac{L_r}{\xi K_1} - \frac{1}{M\xi}\left\{\frac{2K_0}{K_1^2}[\cosh(K_1 L_r) - 1]\right.\right.$$
$$\left.\left. + \frac{1}{K_1}\sinh(K_1 L_r) + \frac{1}{K_0}[\cosh(K_1 L_r) - 1]\left(\frac{1}{\xi K_1} - 1\right)\right\}\right]$$
$$[13]$$

for the Etchenique model, where

$$M = K_0\sinh(K_1 L_r) + K_1\cosh(K_1 L_r),$$

$$K_1^2 = K_0^2 + \xi^{-2} \text{ and } K_0 = \sqrt{j\omega\rho_2/\eta_2}$$

In the case of smooth surfaces ($L_r \to 0$), only the first term remains and the theory of Kanazawa is reproduced.

A new model that makes easier the interpretation of the physical phenomena which happen when a rough surface oscillates in contact with a fluid has been recently introduced by the authors.[15,16] This model characterizes the roughness as a surface of spherical shells whose characteristic dimensions are the height h_r and the radius of the base r_r (Fig. 2). The solution of the linearized Navier-Stokes equation applied to this model enables us to obtain the corresponding drifting force and the acoustic impedance of the rough surface in contact with the liquid as follows

$$Z_2 = \left[3\pi\eta_2(nh_r) + \frac{3}{2}\frac{\eta_2}{\delta_2}\Delta S_r + \frac{\eta_2}{\delta_2}\right.$$
$$\left. + j\omega\left(\frac{3}{4}\rho_2\delta_2\Delta S_r + \frac{1}{2}\rho_2 V_r + \frac{1}{2}\rho_2\delta_2\right)\right] \quad [14]$$

where ΔS_r is the increase of the surface per unit area due to the roughness, in comparison with a flat surface, and V_r is the volume of the roughness per unit area. For the spherical-shell model, the surface and the volume of one shell are $S_r^1 = \pi(h_r^2 + r_r^2)$ and $V_r^1 = \pi h_r(h_r^2 + 3r_r^2)/6$. The increase of the surface due to one shell in relation to a flat surface can be found making $h_r = 0$ and subtracting the result from the total surface. Therefore $\Delta S_r = n\pi h_r^2$ and $V_r = n\pi h_r(h_r^2 + 3r_r^2)/6$, where n is the number of shells per unit area. For a complete coverage (Fig. 2), n can be calculated as the ratio between the unit area and the area of the hexagon in which the base of the shell is inscribed as follows

$$n = 1/(2r_r^2 3^{1/2}) \quad [15]$$

According to Eq. 14, the drifting force per unit area is the sum of two components, one in phase with the oscillating velocity, the loss part, and the other one 90° out of phase, the inertial part. Each one of the parts includes two terms additional to the loss and inertial terms of a flat surface (Kanazawa terms corresponding to the third terms in both parts): in the loss part, a term associated with the

well-known Stokes law and an additional term proportional to the increase of surface due to the roughness (ΔS_r) and inversely proportional to the wave penetration depth (δ_2) in the liquid; in the inertial part the term corresponding to the increase of surface due to the roughness (ΔS_r), which represents the extra mass of liquid displaced by the penetration of the shear wave, generated by the oscillating movement of the extra surface (ΔS_r), into the liquid, and the term corresponding to the mass of liquid displaced by the oscillating movement of the volume of roughness (V_r).

This model can be used to separate roughness and coating mass effects during the gravimetric regime.

Separation of mass and roughness effects at gravimetric regimes.— According to Eq. 14, the effect of the roughness has additive contributions in both real and imaginary parts of Z_2 in relation to the corresponding parts of the acoustic impedance of a flat surface (Kanazawa terms). If one assumes that in the gravimetric regime there are no viscoelastic contributions in the real and imaginary parts of the acoustic load impedance, the changes in the real part will be due to the roughness and the changes in the imaginary part will be due to the mass of the coating and to the extra mass of liquid displaced by the roughness.

In relation to the model of roughness in Fig. 2, when the gravimetric regime is considered, the resonant frequency shift, taken as the difference between the maximum conductance frequencies of the uncoated sensor in contact with liquid and the coated sensor, will have two contributions, one due to the mass density of the coating and the other one due to the mass of liquid per unit area displaced by the roughness, which can be obtained from the imaginary part of Eq. 14.

The surface mass density of the coating, m_p, will be (Fig. 2) the addition of the surface mass density of the rough layer, m_{rp}, and the surface mass density of the uniform coating layer, m_{lp}, formed at the bottom with a thickness h_{lp} ($m_{lp} = \rho_p h_{lp}$, where ρ_p is the density of the polymeric coating layer). In a galvanostatic electrochemical deposition, the coating mass density $m_p = m_{rp} + m_{lp}$ can be estimated from the charge and Faraday law as $m_p = \chi C_F It$, where χ is the efficiency; C_F is the theoretical mass deposited per unit charge, which can be obtained from Faraday law as $C_F = M/(Fn^e)$ with M the molar mass of the monomer, F the Faraday constant (9.6485 C/mol), and n^e the number of electrons exchanged in the chemical reaction, I is the constant current density during the galvanostatic experiment, and t is the time.

The surface mass effect associated with the roughness, Δm^r, can be obtained from the imaginary part of Eq. 14 as follows

$$\Delta m^r = \frac{3}{4}\rho_2\delta_2\Delta S_r + \frac{1}{2}\rho_2 V_r = \frac{1}{2}\frac{\rho_2}{\rho_p}\left(\frac{9\delta_2 h_r}{h_r^2 + 3r_r^2} + 1\right)m_{rp} \quad [16]$$

The surface mass density of the rough layer m_{rp}, from the polymer density and the volume of one shell, is given by

$$m_{rp} = \rho_p V_r = \rho_p n\pi h_r(h_r^2 + 3r_r^2)/6 \quad [17]$$

In gravimetric regimes the surface mass density, m_{SB}, obtained from the Sauerbrey equation $(\Delta f_s|_{coating} = -C_{SB}m_{SB})$ provides the additive contribution of the coating surface mass density and the surface mass effect per unit area due to the roughness as follows

$$m_{SB} = m_p + \Delta m^r \quad [18]$$

The shift in the real part of the acoustic load impedance, in relation to the value for a flat surface, can be expressed as a function of the surface mass density of the rough layer m_{rp} as follows

$$\frac{\Delta R_2}{\omega_0} = \frac{1}{\omega_0}\left(3\pi\eta_2(nh_r) + \frac{3}{2}\frac{\eta_2}{\delta_2}\Delta S_r\right) = \frac{9}{2}\frac{\rho_2}{\rho_p}\left(\frac{2\delta_2^2 + \delta_2 h_r}{h_r^2 + 3r_r^2}\right)m_{rp}$$
$$[19]$$

where ω_0 is the resonant frequency of the compound resonator.

From Eq. 15-19, the characteristic parameters of the roughness h_r and r_r, and the thickness of the uniform coating layer, h_{lp}, can be obtained as a function of ΔR_2, m_{SB}, and m_p, which can be obtained from the experimental magnitudes Y, Δf_s, and I, respectively, as follows

$$h_r = (-b + \sqrt{b^2 + 4c})/2 \qquad [20]$$

$$r_r = \sqrt{Eh_r(2\delta_2^2 + \delta_2 h_r)} \qquad [21]$$

$$m_{rp} = \rho_p \frac{\pi}{2\sqrt{3}} \frac{h_r}{r_r^2}\left(\frac{h_r^2 + 3r_r^2}{6}\right) \qquad [22]$$

$$h_{lp} = \frac{1}{\rho_p}(m_p - m_{rp}) \qquad [23]$$

where b and c have the following expressions

$$b = \frac{6E\delta_2^2 + 9\delta_2 - 9D\delta_2}{3E\delta_2 + 1}, \quad c = \frac{18D\delta_2^2}{3E\delta_2 + 1}$$

with $D = \omega_0/\Delta R_2(m_{SB} - m_p)$ and $E = (9\pi\rho_2/24\sqrt{3}\omega_0/\Delta R_2)$.

Experimental

Chemicals.— In the course of the experiments, the following chemicals were used: EDOT (Baytron M Bayer), tetrabutylammonium perclorate (TBAClO$_4$), and acetonitrile (Merck).

QCR measurements: electrochemical experiments.— A standard three-electrode electrochemical cell was employed with a JAISSLE potentiostat-galvanostat IMP 88. The reference electrode was a Ag/AgCl electrode and all potentials herein are quoted with respect to this reference; a platinum mesh auxiliary electrode was employed.

The electropolymerization solution contained 47 mM EDOT and 0.1 M TBAClO$_4$ in acetonitrile. PEDOT films were deposited galvanostatically, by setting a current density of 212,2 μA cm^{-2}. This current density was chosen in order to obtain a homogeneous PEDOT deposit with good coverage electrode surface.

The working electrode potential was recorded during the galvanostatic polymerization and remained constant during electropolymerization.

Gold coated AT-cut 10 MHz quartz crystals with 14 mm blank diameter and 0.5 cm electrode diameter (International Crystal Manufacturing Company Inc., Oklahoma City, OK, USA; Cat. 31210) were employed. A Teflon cell with two vinyl O-rings was used for sealing the quartz crystal with only one face of the crystal in contact with the electrolyte solution.

QCR sensor admittance spectra, conductance and susceptance, around resonance were acquired with an HP5100A network analyzer interfaced by an IEEE-488 card (National Instruments GPIB PCIIA), with a purpose written software under Labview (National Instruments) environment.[30] The admittance spectra were acquired dynamically during EDOT electropolymerization. Spectra were taken every 1.5 s.

The following conductance and susceptance measurements of the QCR sensor around resonance were performed: (*i*) uncoated crystal in air, (*ii*) uncoated crystal in contact with the liquid electrolyte, and (*iii*) PEDOT film coated crystal in contact with the liquid electrolyte during electropolymerization.

Ellipsometric-SEM-electrochemical experiments.— A SEN-TECH SE 400 variable angle rotating analyzer-type ellipsometer equipped with a He–Ne laser ($\lambda = 632.8$ nm) was used for the ellipsometric experiments. The in situ measurements were carried out in a commercial Teflon cell, whose windows allow only measurements at a fixed angle of 70°. The ellipsometric parameters (Ψ and Δ) were collected during the electropolymerization until the surface of the electrode became dark and no further ellipsometric measurements were possible; the thickness values were obtained using a
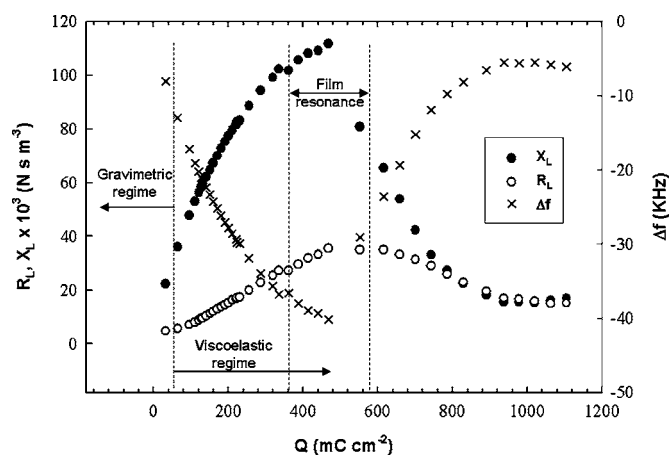
Figure 3. Evolution of the real and imaginary parts R_L and X_L of the acoustic load impedance, Z_L, at angular frequencies ω_1 near the maximum conductance.

simple three-layer model (substrate/film/acetonitrile solution) for constant optical properties. Gold evaporated on silicon wafers was used as a substrate, with 20 nm of titanium and 200 nm of gold.

Scanning electron microscopy (SEM) investigations were also performed with a Philips XL30 CP SEM.

Results

Sensor calibration.— Admittance spectra measurements of the uncoated crystal in air and in contact with the electrolyte solution around resonance were used for sensor calibration.

The density of the solution was estimated from the literature, through the density of the acetonitrile (0.777 g cm^{-3}) and the mass of TBAClO$_4$ in dissolution, assuming nonincrease in volume, to be $\rho_2 = 0.805$ g cm^{-3}.

The viscosity of the semi-infinite Newtonian medium was taken from the literature as the viscosity of the acetonitrile: $\eta_2 = 0.369$ mPa s.[31]

From the calculated density and viscosity, the characteristic acoustic impedance of the semi-infinite medium results, $Z_2 = 3053(1 + j)$N $\times$ s $\times$ m^{-3}.

The sensor calibration parameters were obtained, through a purpose-developed algorithm described elsewhere,[24,26] to assure the best fitting between the conductance spectrum computed by the TLM for the uncoated sensor in contact with the liquid, whose characteristic impedance was assumed to be the one previously calculated, and the corresponding spectrum experimentally measured. The obtained calibration parameters were

$$h_q^{ef} = 166.315 \ \mu m, \quad C_0^{ef} = 4.66 \ pF,$$

$$\eta_q^{ef} = 0.1948 \ Pa \ s, \quad and \quad C_{ex} = 6.93 \ pF$$

Acoustic load impedance: acoustic regimes.— Once the calibration parameters have been obtained, the acoustic load impedance, $Z_L(\omega_1)|_{exp}$, can be solved, as a function of the experimental admittance, from Eq. 1 and 2. The acoustic load impedance at the frequency ω_1 corresponding to the conductance peak of each acquired conductance spectrum was calculated. The real and imaginary parts, R_L and X_L, along with the frequency shift between the conductance peaks of the coated sensor in contact with the medium and the uncoated sensor, are represented in Fig. 3 for characterizing the electropolymerization process; as can be observed, the frequency shift, Δf, follows nearly the opposite evolution to the imaginary part of the acoustic load impedance, as can be understood through the acoustic load approximation expression[18]: $X_L \approx -k\Delta f$, where $k \approx 3$ for a 10 MHz AT-cut QCR such as the one described in the section QCR measurements: electrochemical experiments.
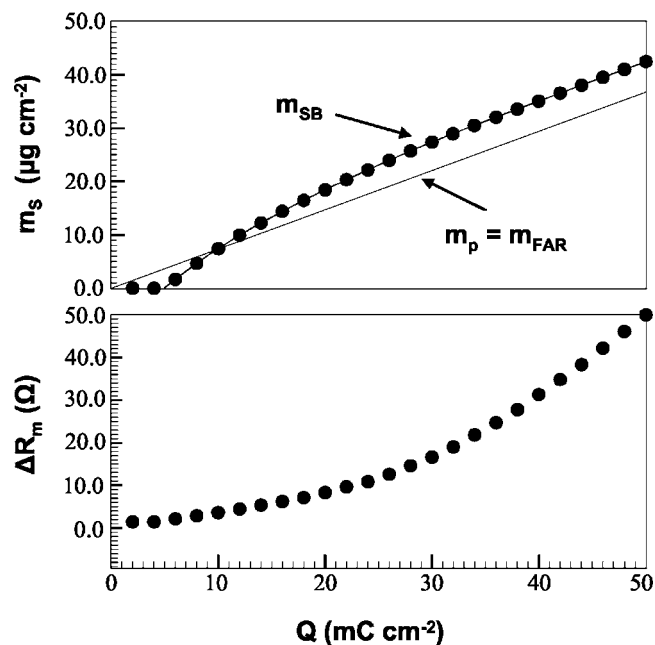
Figure 4. Detail of the evolution of the mass density corresponding to the Sauerbrey equation and of the shift in the reciprocal of the maximum conductance (motional resistance shift) up to 50 mC cm^{-2} charge density.

Figure 3 shows that the coating passes through different acoustic regimes: gravimetric or Sauerbrey-like regime and viscoelastic regime.

Gravimetric regime.— Figure 4 shows a detailed representation of the initial times ($Q < 50$ mC cm$^{-2} - t < 235$ s), where one could assume gravimetric regime. The surface mass density, m_{SB}, obtained with the Sauerbrey equation (see Eq. 9 and 18) starting from the corresponding frequency shifts is represented in the upper panel along with the theoretical mass density, $m_p = m_{Far}$ (Eq. 24), obtained from Faraday law as $m_{Far} = \chi C_F Q$, where Q is the charge density and $C_F = 0.737$ mg/C for the 3,4-ethylendioxythiophene, whose molar mass $M = 142.2$ g/mol, and the efficiency has been assumed to be 1; the resistance shifts taken as the difference in the reciprocal of maximum conductance magnitudes between the coated and uncoated device in contact with the liquid are represented in the lower panel

$$m_{Far}(\text{g cm}^{-2}) = 0.0737 \times 10^{-5} Q(\text{mC cm}^{-2}) \qquad [24]$$

The sensor response is characterized in the initial times for an important increase of X_L (decrease of Δf) in comparison with the increase of R_L. This behavior could correspond, in principle, to a gravimetric regime where the frequency shifts could be directly related to the polymer mass through the Sauerbrey equation (Eq. 9); however, some considerations should be done and carefully considered. For some authors, the gravimetric regime is the one where there is not a change in the resistance shift.[7] It should be more rigorously stated that the acoustic gravimetric regime occurs when the viscoelastic properties of the coating are not reflected on the sensor response. In some cases one can obtain resistance changes due to contributions different from viscoelastic effects[14] and the sensor can follow working in the gravimetric regime, even with changes in the resistance. This can happen, for instance, when a rough surface coating is being deposited. This aspect is discussed later on.

Viscoelastic regimes.— As the time increases ($t > 235$ s $- Q > 50$ mC cm^{-2}) the acoustic load impedance shows a further increase of X_L (a further decrease of Δf) and an important increase of R_L, that is, a decrease of the conductance peak (Fig. 3). It means that the coating is getting thicker and the contribution of its viscoelastic
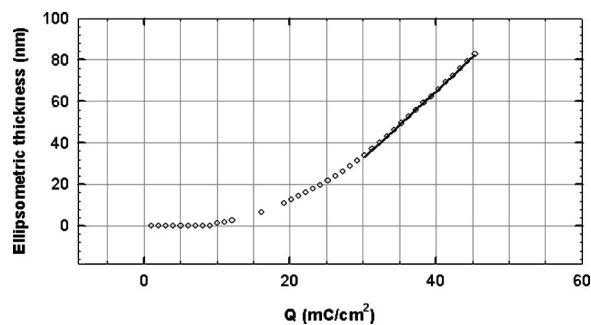
Figure 5. Measured ellipsometric thickness as a function of the charge density.

properties on the sensor response is not negligible; the loading effects on R_L are comparable to the effects on X_L, the sensor response is highly damped, and the frequency shift (the change in X_L) can no longer be directly related to the coating mass.

Figure 3 shows that during the viscoelastic regime, the acoustic load resistance reaches a maximum after around 500 mC cm^{-2} and then decreases while the resonant frequency shift shows a minimum with a later frequency increase. This behavior is similar to that of a film mechanical resonance, however a further analysis is necessary to assure that this effect happens. Typical film mechanical resonances show a very abrupt frequency shift after reaching the minimum, which normally reaches positive values; in Fig. 3 the frequency shift does not change in sign, but film mechanical resonances without positive frequency shifts can be observed for coatings of $G' = G'' = 1$ or 0.1 MPa in contact with liquid. In fact, the main characteristic which defines the film mechanical resonance is that the wave phase shift across the film must be $\pi/2$, that is, the thickness of the film must be equal to a quarter of the acoustic wavelength[32]; in order to clarify this aspect and to evaluate the viscoelastic properties of the PEDOT during the electropolymerization process, the extraction of the coating properties along with a further analysis is necessary.

Ellipsometric results.— The ellipsometric thickness measured during PEDOT galvanostatic deposition as a function of the applied charge density has been represented in Fig. 5. This thickness shows a linear growth (Eq. 25) between 30 and 45 mC cm^{-2} of applied charge density. For charge densities smaller than 30 mC cm^{-2} the ellipsometric thickness does not show a linear growth. Either very thin layers for the thickness resolution of the system or the probable nonuniform deposition make the measurements of the ellipsometric thickness not very reliable during the initial times. For charge densities greater than 50 mC cm^{-2}, the ellipsometric thickness cannot be measured due to a considerable light absorption at 632.8 nm. Values of ellipsometric thickness for higher charge densities can be extrapolated from Eq. 25 if one assumes this constant growth

$$h_1(\text{nm}) = -64.6972 + 3.2423 Q \qquad [25]$$

where Q is the charge density in mC cm^{-2}.

Roughness effects.— SEM studies of polymer samples performed at different values of electropolymerization charge density (Fig. 6) revealed changes in the surface morphology of the PEDOT during the deposition. Figure 6 seems to indicate that the surface of the coating is getting more compact as the charge density grows.

Values of the viscoelastic properties G_1' and G_1'' in the MPa range have been reported for the related conducting polymer poly(3-methyl-thiophene) by Hillmann et al.[8,33] These authors have described a nonmonotonous dependence of the viscoelastic properties of the coating G_1' and G_1'' with polymerization charge. The fact that two material properties, G_1' and G_1'', turn out to be dependent on the film electropolymerization charge (assumed at first proportional to
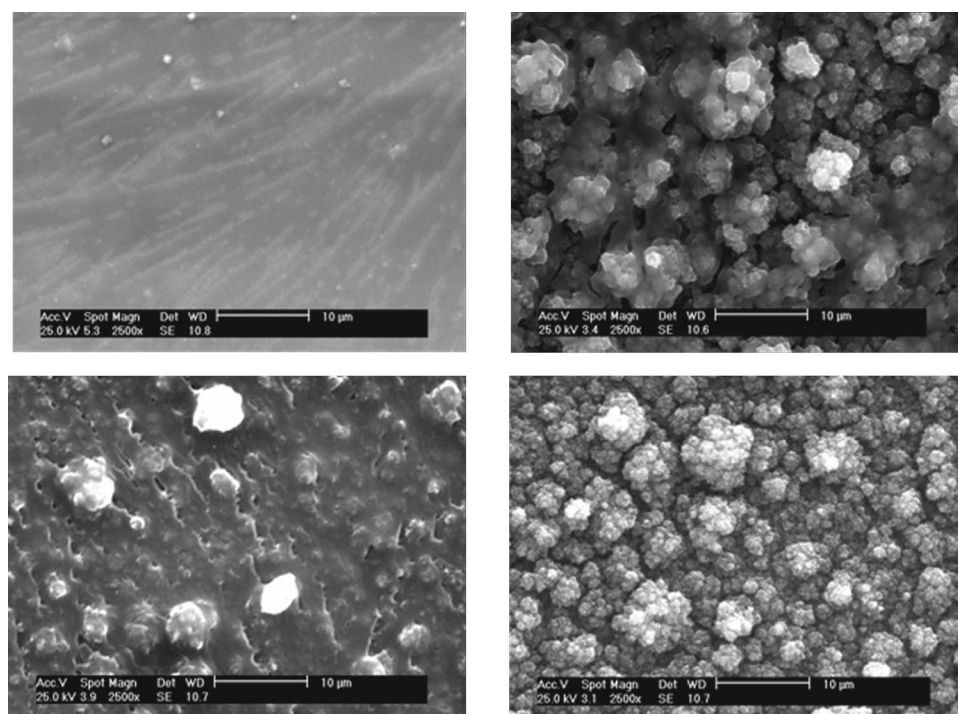
Figure 6. SEMs of PEDOT films prepared on Au electrode of a quartz taken at different charge densities: 12–20 mC cm^{-2} (upper left panel); 200 mC cm^{-2} (lower left panel); 400 mC cm^{-2} (upper right panel); and 900 mC cm^{-2} (lower right panel).

the film thickness) deserves some careful consideration. The viscoelastic properties extracted at different charge densities are obtained making use of the oversimplified model in Fig. 1a, which assumes constant density and shear moduli of a coating whose thickness increases with the applied electrical charge. A more realistic view is that the film structure evolves during film growth and one should expect the contribution of other factors on the effective viscoelastic properties extracted following the simplified model in Fig. 1a. Among those factors, the film roughness is considered in the next section.

Discussion

Mass density, surface roughness, and efficiency at gravimetric regimes.— As outlined above, calculation of the polymer mass through the Sauerbrey equation should be possible during the gravimetric regime and a good match should be expected between this mass and the theoretical one obtained from Faraday law with a specific efficiency (Eq. 24). However, as can be observed in Fig. 4, the sensor does not detect mass during the first seconds of the electropolymerization process, and when the mass is detected the slopes of the mass gain are found to be around a factor of 2 bigger than those predicted by the Faraday law for an efficiency of 100%. A later decrease of the mass gain slope is predicted by the Sauerbrey equation; from 30 to 50 mC cm^{-2} polymerization charge density, the Sauerbrey mass has a lineal evolution (Eq. 26) with a slope very close to that of the faradaic mass. Almost the same effect has been recently reported by Bund in a potenciostatic electrodeposition of PEDOT[14]

$$m_{SB}(\text{g cm}^{-2}) = 0.452 \times 10^{-5} + 0.0742 \times 10^{-5} Q(\text{mC cm}^{-2})$$

[26]

The absence of mass detection during the first seconds of the electropolymerization process can be due to the mechanism of oxidative electropolymerization of thiophenes that, like in the polymerization of pyrrole, proceeds via radical cationic coupling resulting in oligomers with 2.5 linkage.[34,35] Therefore, at short times soluble thiophene oxidation intermediates and short chain oligomers formed in a precursor step can diffuse away from the electrode and result in electrical charge lost into solution with no mass gain contribution. At longer times, oligomers of sufficient length are produced and

precipitate onto the electrode surface giving rise to nucleation phenomena,[36] which are reflected on the sensor response.

The precipitation of the first oligomers onto the quartz surface could explain the greater slopes in the mass gain predicted by the Sauerbrey equation in comparison with the theoretical one derived from Faraday law; however, additional effects remain because an extra mass is predicted by the Sauerbrey equation (Fig. 4).

Effectively, an acoustically thin film is supposed to be a homogeneous coating uniformly deposited on the sensor surface with a flat surface in contact with the liquid. Therefore, there is no extra contribution of the liquid on the sensor response in comparison with an uncoated sensor in contact with the liquid, because the liquid interface sees the same flat surface moving synchronously (acoustically thin) with the quartz surface; the only extra contribution is the inertial contribution associated with the surface mass of the film. If the nucleation phenomenon previously described leads to a nonhomogeneous deposition, where small polymer nuclei were spread on the surface leaving voids filled with the liquid, the interface with the liquid is not flat and extra contributions exist. The main contribution is inertial due to the extra volume of liquid displaced by the roughness and the sensor response could be mainly dominated by the imaginary part X_L, but also a small effect on the real part R_L could arise. If one assumes that the differences between the Sauerbrey prediction and the Faraday mass until a 50 mC cm^{-2} polymerization charge density are due to the roughness, the application of Eq. 15-19 allows obtaining the roughness characteristic parameters according to the model depicted in Fig. 2. The results are represented in Fig. 7 and 8. Figure 7 shows the evolution of the characteristic parameters of the roughness, r_r and h_r, along with the thickness of the uniform bottom layer h_{lp}; the maximum uniform thickness of the bottom layer $h_{lp\text{-max}}$ obtained when all the Faraday mass is assumed to be uniformly deposited is included for comparison ($h_{lp\text{-max}} = m_{\text{Far}}/\rho_p$, where a polymer density of $\rho_p = 1.5$ g cm^{-3} has been taken from the literature[37]). The evolution of the roughness parameters [one must bear in mind that they are average values for the case of a complete coverage (Fig. 2)] indicates that in the beginning the coating is formed by a small thickness uniform layer with relatively big mountains on top ($r_r \approx 200$ nm, $h_r \approx 100$ nm, and $h_{lp} \approx 50$ nm). As the coating grows, the uniform bottom layer gets thicker and the parameters of the rough layer, both r_r and h_r, decrease, making the poly-
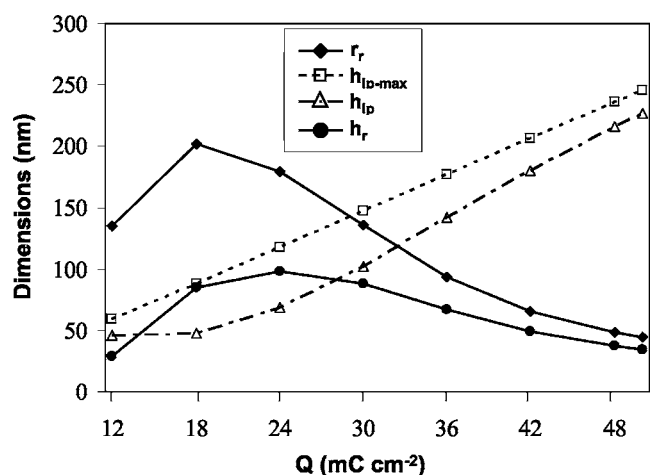
Figure 7. Evolution of the roughness dimensions according to the spherical shell roughness model depicted in Fig. 2, for the experimental data given in Fig. 4.

Figure 8. Evolution of the different mass contributions, during the gravimetric regime in Fig. 4, associated with a rough coating.

mer layer more compact ($r_r \approx 45$ nm, $h_r \approx 35$ nm, and $h_{lp} \approx 227$ nm); the effect of the roughness decreases as the polymer grows but maintains a non-negligible effect in the charge density interval considered. This can be observed in Fig. 8 where the mass densities predicted by Sauerbrey and Faraday law are represented along with the mass density of the uniform layer, m_{lp}, the mass density of the rough layer, m_{rp}, and the mass effect due to the roughness, Δm^r. Figure 8 shows that the mass effect due to roughness maintain its absolute value, but its relative weight in relation to the real mass diminishes with the polymer growth. For 50 mC cm^{-2} polymer charge density the relative weight of the roughness mass effect is 13% in relation to the Faraday mass.

This analysis indicates that the mass obtained from the Sauerbrey equation, including the roughness effect, agrees well with the Faraday mass for a 100% efficiency, at least in the polymerization charge density range considered. Efimov et al.[38] also report current efficiencies of 100% for PEDOT electropolymerization up to mass densities of 30–40 μg cm^{-2}. Bund and Schneider's results showed that the current efficiency of a potentiostatic PEDOT electropolymerization (0.1 M EDT, 0.1 M LiClO$_4$ in acetonitrile) remains at 100% up to mass densities of 100 μg cm^{-2}, which corresponds with a charge densityof 74 mC cm^{-2} in our experiment.[14]

As the polymer coating gets thicker, its viscoelastic properties influence the sensor response and both roughness and viscoelastic contributions exist. The analysis of the viscoelastic properties of the coating and the effect of the roughness during viscoelastic acoustic regime is more complex and this is performed and discussed in two steps: first, the algorithm for coating parameter extraction outlined above is used for evaluating the effective properties of the coating following the model depicted in Fig. 1a; and second, the effect of the roughness on the effective viscoelastic properties of the coating is evaluated by means of the same algorithm but used, in this case, as a simulation tool.

Effective mass density and effective viscoelastic properties of the coating.— The third step of the algorithm described in the beginning of this article was applied, and provided the set of possible triads of coating properties, which are a solution of the problem of parameter extraction, for each couple of R_L and X_L in Fig. 3, and are found before the first film mechanical resonance and between the first and second film resonances. Then, the fourth step had to be applied for the selection of the appropriate triad for each value of Z_L. In all cases, the fitting error between the experimental conductance spectrum and the one derived from the TLM for the optimum triad made unfeasible the application of the fitting restriction; the experimental and theoretical spectra only matched near the maximum con-
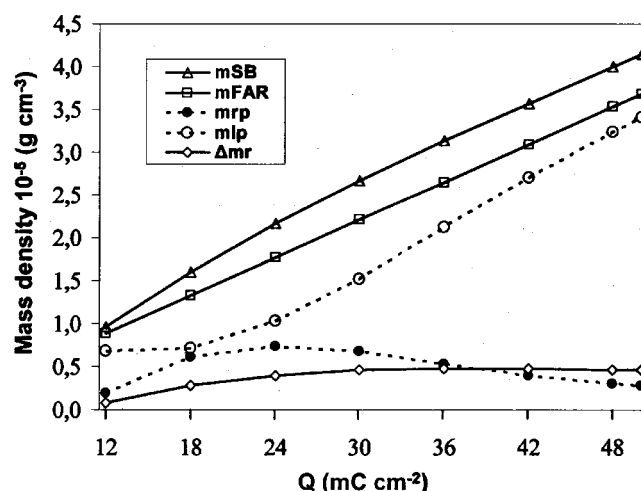
ductance and the level of matching decreased as one went near the wings, and then additional restrictions had to be used for the extraction of the appropriate triad. Four different additional restrictions were initially applied for the selection of the triad: (*i*) Sauerbrey mass restriction where the algorithm selected the triad whose mass density was the nearest to the Sauerbrey mass derived from Eq. 26; (*ii*) Faraday mass restriction where the algorithm selected the triad whose mass density was the nearest to the Faraday mass derived from Eq. 24; (*iii*) ellipsometry mass restriction where the algorithm selected the triad whose mass density was the nearest to the mass derived from the ellipsometric thickness extrapolated from Eq. 25 and the polymer bulk density taken from the literature (1.5 g cm^{-3});[37] and (*iv*) the non-mass-loss restriction where the physical condition that the coating cannot lose mass was imposed to the algorithm for the selection of the triad. This is a much softer restriction than the previous ones. The results are shown in Table II and Fig. 9, 10, and 11, for Faraday mass, ellipsometry mass, and non-mass-loss restrictions, respectively; Sauerbrey mass restriction provided results almost identical to Faraday mass restriction, and it is not shown.

Black symbols (square and circular) represented in the figures indicate that the triad whose mass density is the nearest to the mass density of the corresponding restriction was found before the first film resonance and white symbols indicate that it was found between the first and second film resonance.

For the Faraday restriction, triads whose mass densities matched almost perfectly the Faraday mass were found practically in all the charge density range, except for the charge density range between 128 and 256 mC cm^{-2} where a loss in efficiency was observed (11 and 33%, respectively—see the fifth column in Table II). It is also worthwhile to indicate that the film resonance arose with the Faraday restriction before it was expected, because triads after first film resonance were found before the film resonance range marked on Fig. 9 (see also Fig. 3). With regard to the effective viscoelastic properties extracted, the analysis showed an important dispersion in the values of the properties up to a charge density of 128 mC cm^{-2} (columns 6–7 in Table II), probably due to the proximity to the gravimetric regime; in this range we should be more confident with the obtained mass densities than with the extracted viscoelastic properties. In the charge density range from 128 to 256 mC cm^{-2}, the effective viscoelastic properties extracted maintained a relatively constant magnitude (G_1' between 0.5 and 1 MPa and G_1'' between 6.8 and 8.5 MPa; see columns 6–7 in Table II). The sharp decrease in the loss shear modulus near before and during the resonance range can be explained as an artifact due to the great noise of the acquired conductance spectra during this range; however, the significant de-

Table II. Theoretical mass density values and extracted coating properties for Faraday, ellipsometry, and non-mass-loss restrictions.

Q (mC cm^{-2})	m_{far} (μg cm^{-2}) (Eq. 24)	$m_{ellip.}$ (μg cm^{-2}) (Eq. 25)[a]	m_S (μg cm^{-2}) F. R.[b]	Effic. (%)[c] F.R.[b]	G'_1 (MPa) F. R.[b]	G''_1 (MPa) F. R.[b]	m_S (μg cm^{-2}) E.R.[d]	G'_1 (MPa) E. R.	G''_1 (MPa) E. R.	m_S (μg cm^{-2}) NML R.[e]	Effic. (%)[c] NML R[e]	G'_1 (MPa) NML R[e]	G''_1 (MPa) NML R[e]
33	24.2	6.2	24.2	0.0	0.55	0.001	24.2	0.55	0.001	29.7	22.9	0.01	1.25
65	47.9	21.9	47.8	0.0	2.06	2.27	39.4	0.91	0.001	50.8	6.2	0.11	3.45
96	71.1	37.2	69.3	−2.5	0.06	5.14	49.1	1.02	0.001	69.3	−2.5	0.06	5.14
128	94.5	52.7	84.2	−10.9	0.89	6.86	56.5	1.12	0.001	84.2	−10.9	0.89	6.86
160	118.0	68.2	97.0	−17.8	0.92	7.43	68.2	1.69	0.18	97.0	−17.8	0.92	7.43
192	141.5	83.6	108.3	−23.4	0.86	7.58	83.7	2.82	0.95	108.3	−23.4	0.86	7.58
224	164.9	99.1	119.0	−27.8	0.48	8.46	99.1	4.14	2.67	119.0	−27.8	0.48	8.46
256	188.5	114.7	126.7	−32.8	0.55	8.54	114.7	4.04	5.91	126.7	−32.8	0.55	8.54
287	211.8	130.1	after first film resonance				130.3	1.71	8.54	134.8	−36.4	0.21	8.89
320	235.3	145.6	after first film resonance				138.6	0.66	8.98	138.6	−41.1	0.66	8.98

[a] The thickness in Eq. 25 is multiplied by the bulk density (1.5 g cm^{-3}) to obtain the mass density.

[b] F.R. = Faraday restriction.

[c] The efficiency loss is calculated in relation to Faraday mass density for an efficiency of 100% (Eq. 24, 2nd column).

[d] E.R. = ellipsometry restriction.

[e] NML R = non-mass-loss restriction.

crease in the loss shear modulus was maintained after the film resonance and until the end of the polymerization with a very constant value around 0.7 MPa and it requires an additional justification, which will be made in the next section. The monotonous increase of the shear storage modulus was linked to the restriction imposed to the algorithm for the selection of the triad which better matched the Faraday mass density given by Eq. 24. This is better understood by comparing with the results of the ellipsometry and non-mass-loss restrictions.

In Fig. 10, the properties extracted from the ellipsometric mass restriction showed a similar trend after the film resonance range as in the Faraday mass restriction, but some important differences can be found before the film resonance range which must be discussed.
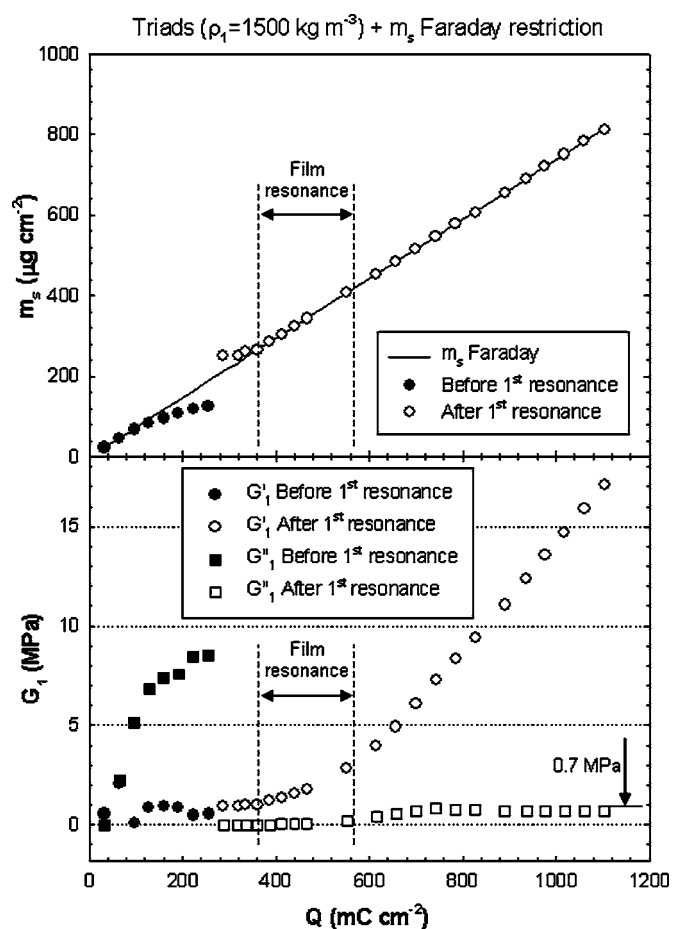

Figure 9. Evolution of the effective coating properties extracted by the algorithm with the Faraday mass density restriction.
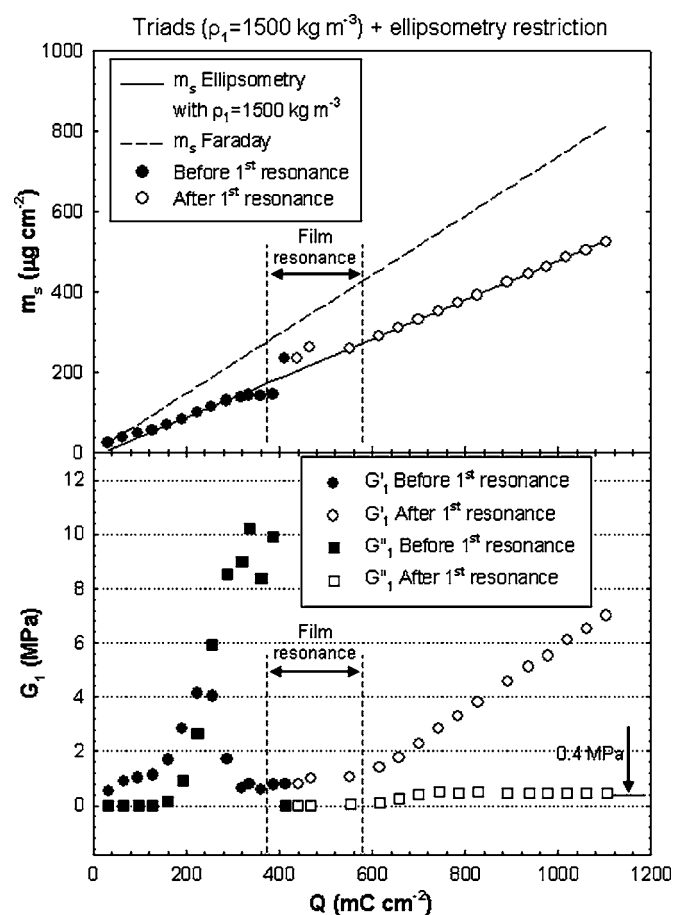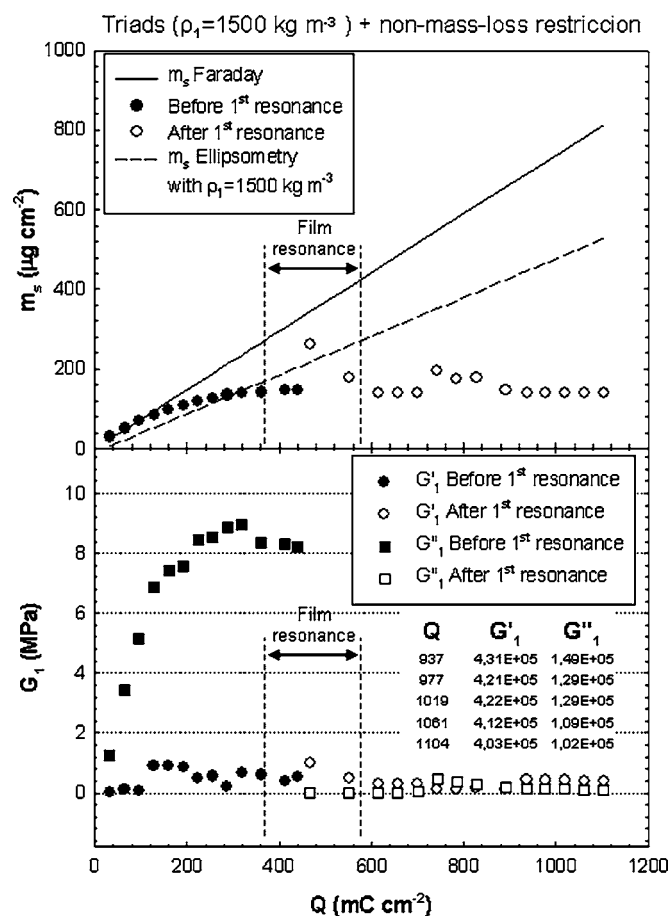

Figure 10. Evolution of the effective coating properties extracted by the algorithm with the ellipsometric mass density restriction.

Figure 11. Evolution of the effective coating properties extracted by the algorithm with the non-mass-loss restriction.

As can be observed, for charge densities smaller than 160 mC cm^{-2} there were no triads whose mass densities perfectly matched the ellipsometric mass densities (compare columns 3 and 8 in Table II). This is a very important fact because it indicates that in this experiment the ellipsometry mass disagrees with the acoustic mass density; it is a well-known fact that the thickness measured by ellipsometry underestimates the acoustic thickness,[39,40] and this disagreement was confirmed in the experiment. Furthermore, in the gravimetric regime (33 mC cm^{-2} in Table II) the triad whose mass density was the nearest to the ellipsometric mass condition had a mass density perfectly matched with the one predicted by Faraday restriction (compare columns 2 and 8 in Table II). The apparent repetitiveness of the viscoelastic properties during this initial charge density range (see Fig. 10) is an indication that the condition imposed by the ellipsometric restriction cannot be found in the physical range of properties considered; in that case the algorithm will provide the lowest value for G_1'' in the physical range considered (see column 10 in Table II). In the charge density range from 160 to 287 mC cm^{-2}, the viscoelastic properties showed a greater dispersion (G_1' between 1.6 and 4.1 MPa and G_1'' between 0.2 and

8.5 MPa; see columns 9–10 in Table II) in comparison with the Faraday restriction in the same charge density range. In the charge density range just before the film resonance range (320–390 mC cm^{-2}; in Table II the one corresponding to 320 mC cm^{-2} is only shown) the effective viscoelastic properties of the coating recovered similar values to those in the Faraday restriction just before resonance (G_1' between 0.6 and 0.8 MPa and G_1'' between 8 and 10 MPa). Everything happens as if the evolution of the effective viscoelastic properties extracted with the ellipsometric restriction was delayed in relation to that of the Faraday restriction. This seems to be confirmed when one observes the evolution of the viscoelastic properties for the ellipsometric restriction after the film resonance range; it follows again the same trend delayed. In order to avoid this dependency, a fourth restrictive condition was imposed which can now be better understood.

Figure 11 and columns 11–14 in Table II show the evolution of the effective properties of the coating when the non-mass-loss restriction was applied. In the charge density range from 33 to 320 mC cm^{-2} (range shown in Table II), the algorithm selected the triads for the best matching to the experimental conductance spectra with the only physical condition that the mass density was equal to or greater than the one selected for the previous charge density. Because of the very noisy conductance spectra near film resonance, for the charge density interval from 320 mC cm^{-2} to the end of the process, the algorithm selects those triads for the best matching to the experimental conductance spectra with the only physical condition that the mass density was equal to or greater than the one that was selected for the 320 mC cm^{-2} charge density.

As can be observed in the gravimetric regime (33 and 65 mC cm^{-2}; compare columns 4 and 5 with 11 and 12, respectively, in Table II), the non-mass-loss restriction predicts an overestimation in the mass density in relation to the Faraday mass restriction. This overestimation perfectly matched with the Sauerbrey prediction; this effect has been treated in a previous section as a consequence of the important contribution of the roughness in the initial times.

In the charge density range from 96 to 260 mC cm^{-2}, the evolution of the effective properties of the coating with the non-mass-loss restriction reproduced exactly the same evolution as that of Faraday mass restriction (compare columns 4, 5, 6, and 7 with 11, 12, 13, and 14, respectively). However, in contrast with what happened in Faraday restriction, the range in which the algorithm found triads before the first resonance was extended and the pass through the first film resonance was obtained by the algorithm where it was expected (see Fig. 3 and 11). At the same time, a significant decrease in the shear loss modulus was observed when passing through the suspected film resonance range while the shear storage modulus maintained a relatively stable value. After the film resonance, the algorithm followed finding the best triad after the first film resonance but without a significant increase in the mass density, and with a significant stability in the shear loss and shear storage modulus around 0.42 MPa for G_1' and 0.12 MPa for G_1''.

If one accepts that saturation in the mass density can occur, the results obtained with the non-mass-loss restriction are coherent in the sense that one expects stable values for the components of the shear modulus once the coating has reached enough thickness and homogeneity. In order to evaluate the degree of validity in the evolution of the effective properties of the coating predicted by the algorithm with the non-mass-loss restriction, an analysis of the

Table III. Error propagation analysis in the viscoelastic properties, indicated as the range of possible properties which can be solutions of the problem of parameter extraction, for an estimated error in the optimum mass density provided by the algorithm for 96, 224, and 1061 mC cm^{-2}.

96 mC cm^{-2}		224 mC cm^{-2}		1061 mC cm^{-2}	
G_1' (MPa) (Error m_s 10%)	G_1'' (MPa) (Error m_s 10%)	G_1' (MPa) (Error m_s 10%)	G_1'' (MPa) (Error m_s 10%)	G_1' (MPa) (Error m_s 80%)	G_1'' (MPa) (Error m_s 80%)
0.001 to 3	2 to 5	0.5 to 4.5	5 to 8.5	0.4 to 1.4	0.11 to 0.21

Table IV. Values for the thickness of the compact layer h_1, and characteristics parameters of the rough layer according to the model in Fig. 1b, L_1, and ξ for different instants during a potentiostatic polymerization of PEDOT (taken from Bund and Schneider[14]).

		Instant 1	Instant 2	Instant 3	Instant 4	Instant 5	Instant 6
I	h_1 (nm)	60	160	300	480	700	1080
	L_r (nm)	140	240	300	320	300	120
	ξ (nm)	35	48	50	52	60	65
D	h_1 (nm)	60	160	300	480	700	1080
	L_r (nm)	140	240	300	320	300	120
	ξ (nm)	65	60	52	50	48	35

propagating error was performed by means of the same algorithm in representative instants of the electropolymerization process.

For a 96 mC cm^{-2} charge density, the propagating error in the viscoelastic properties due to a small error in the extracted mass density of the coating is very large, because the possible values of the shear loss modules for an acceptable error of 10% in the extracted mass density are in the range of 2–5 MPa (see Table III). This means that the coating is very near the gravimetric behavior and one must be confident in the value of the mass density extracted but the values of the extracted viscoelastic properties must be treated with skepticism.

The analysis of the propagation error in viscoelastic properties for a 224 mC cm^{-2} charge shows that if an error of 10% is assumed to be acceptable in the mass density, the range of possible values for the shear loss modulus continues staying higher than the value obtained after the resonance (from 5 to 8.5 MPa; see Table III). Therefore, it means that the decrease of the shear loss modules when passing through the film resonance interval is not due to an artifact; an explanation of this effect is given below.

The analysis of the propagation error in the viscoelastic properties for a 1061 mC cm^{-2} charge density shows that even a big error as much as 80% in the mass density extracted would only provide deviations in the shear loss and shear storage modulus ranged between 0.4 and 1.4 MPa for G_1' and 0.11 and 0.21 for G_1'' (see Table III). This means that the viscoelastic properties extracted at the end of the process are relatively independent of the mass density up to increments in the mass density as much as 80%.

After this discussion, if the evolution of the coating viscoelastic properties extracted by the algorithm with the non-mass-loss restriction are accepted as valid in their orders of magnitude, and the coating mass density does not show a significant increase when passing through the suspected resonance interval, it is necessary to explain the change in the coating properties which are responsible for the change in the surface acoustic impedance and cause the coating to pass through a film resonance.

A possible explanation is that in the beginning of the polymerization the coating is formed by polymer nuclei with big cavities filled with solvent, then the viscoelasticity is dominated by the shear loss modulus because the viscosity of the solvent takes an important role. As the polymerization develops it seems to be coherent, according to the results of the SEM (Fig. 6a-d), that the coating is getting more compact and the voids filled with solvent are replaced by polymer; then the role of the viscosity (shear loss modulus) diminishes at the same time as the rigidity of the coating arises; additionally a reduction of the mass density gain could happen due to the replacement of the trapped solvent molecules in the voids by those of the polymer. In the next section the effect of a change in the coating roughness morphology on the effective viscoelastic properties of the coating is analyzed.

Contribution of the roughness on the effective viscoelastic properties of the coating.— The algorithm of coating properties extraction referred to in the first subsection of the article can be used as a tool for analyzing the contribution of the roughness on the viscoelastic properties of the coating in the nongravimetric regime. For that, the model depicted in Fig. 1b was used to represent the compound

resonator. The acoustic impedance Z_2 of the rough layer in contact with the liquid was derived from Daikhin and Urback, and Etchenique models[11,19] for a set of characteristic parameters of the rough layer h_1, L_r, and ξ taken from experimental data reported by Bund and Schneider for a potentiostatic polymerization of PEDOT in acetonitrile at different instants (Table IV).[12,14] The set of parameters considers two different evolutions of the porosity ξ (I, increasing or D, decreasing) while maintaining the same evolution in the characteristic height of the roughness L_r. Viscoelastic properties for the compact layer of the coating were selected in the range of those obtained above for the non-mass-loss restriction as $G_1' = 1$ MPa and $G_1'' = 0.1$ MPa.

Once Z_2 was obtained, the TLM (Eq. 1) could be used, with typical parameters of a 10 MHz AT-QCR (Table I) to simulate the
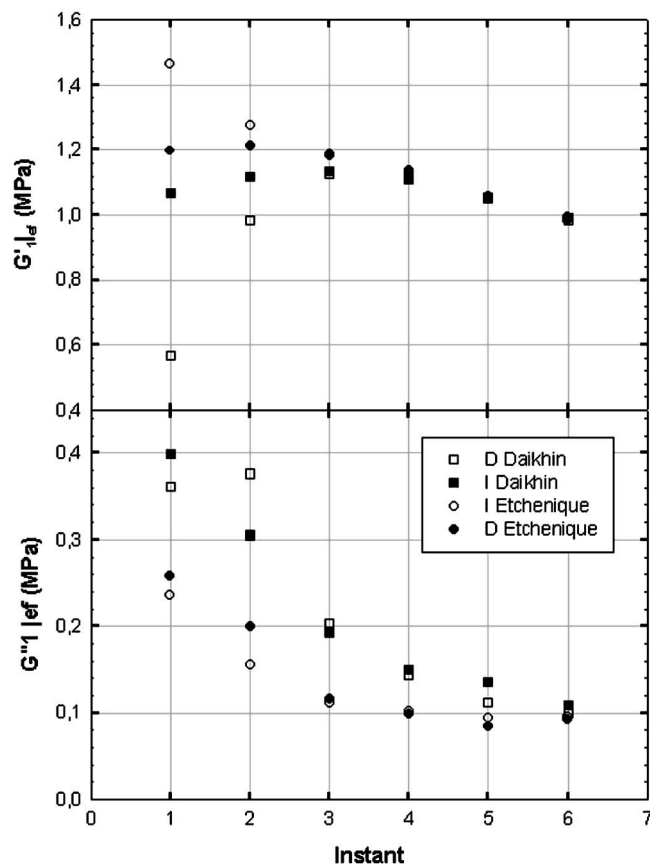
Figure 12. Evolution of the effective viscoelastic properties of a coating extracted by the algorithm starting from simulated experimental data corresponding to a coated QCR according to the roughness model depicted in Fig. 1b with values of the thickness of the compact layer h_1 and the characteristic parameters of the roughness L_r, ξ given in Table IV. The original viscoelastic values for the compact layer were: $G_1' = 1$ MPa and $G_1'' = 0.1$ MPa.

conductance and susceptance spectra at the different instants in Table IV. The obtained conductance spectra were used as experimental input data for the algorithm. Because the experimental data were obtained by simulation from the TLM ("theoretical conditions"), the fitting condition in the fourth step of the algorithm could be applied and the effective viscoelastic properties of the coating, according to the model depicted in Fig. 1a, were extracted with negligible error (Fig. 12)[26]; a test of that is the recovery of the original viscoelastic properties of the compact layer when the roughness disappears.

Figure 12 shows the effect of the evolution of the roughness in Table IV in the effective viscoelastic properties of the coating. As can be observed, the models of Daikhin and Urbakh, and Etchenique, for an increasing and decreasing porosity, respectively, predicted a nonsignificant change in the shear storage modulus whose evolution is maintained relatively stable around the original value of the compact layer, and a significant decrease in the magnitude of the shear loss modulus. This agrees well with what happened during the analysis made above for the non-mass-loss restriction.

Conclusion

This work shows that changes in the surface morphology of the coating during EQCM experiments should be taken into account for an appropriate characterization of the polymerization process. The surface roughness contributes to the sensor response in both gravimetric and viscoelastic regimes. At gravimetric regimes, the effect of the roughness could produce changes in the maximum conductance frequency shift as well as in the conductance peak (motional resistance), which can lead to a misinterpretation of the Sauerbrey mass gain. At viscoelastic regimes, the effect of the roughness appears as a change in the effective properties of the coating, mainly in the effective viscoelastic properties. This change in the effective properties of the equivalent uniform coating layer, near the film resonance thickness, can cause the coating layer to pass through the film resonance phenomenon.

Acknowledgments

References

1. A. C. Arias, M. Granström, D. S. Thomas, K. Petritsh, and R. H. Friend, *Phys. Rev. B*, **60**, 1854 (1999).
2. B. Piro, L. A. Dang, M. C. Pham, S. Fabiano, and C. Tran-Minh, *J. Electroanal. Chem.*, **512**, 101 (2001).
3. L. Goenendaal, F. Jonas, D. Freitag, H. Pielartzik, and J. R. Rynolds, *Adv. Mater. (Weinham, Ger.)*, **12**, 481 (2000).
4. U. Rammelt, P. T. Nguyen, and W. Plieth, *Electrochim. Acta*, **46**, 4251 (2001).
5. A. R. Hillman, *Solid State Ionics*, **94**, 151 (1997).
6. H. L. Bandey, A. R. Hillman, M. J. Brown, and S. J. Martin, *Faraday Discuss.*, **107**, 105 (1997).
7. A. R. Hillman, A. Jackson, and S. J. Martin, *Anal. Chem.*, **73**, 540 (2001).
8. M. Skompska, A. Jackson, and R. Hillman, *Anal. Chem.*, **72**, 4748 (2000).
9. A. R. Hillman, M. J. Brown, and S. J. Martin, *J. Am. Chem. Soc.*, **120**, 12968 (1998).
10. C. Kvarnström, H. Neugebauer, S. Blomquist, H. J. Ahonen, J. Kankare, and A. Ivaska, *Electrochim. Acta*, **44**, 2739 (1999).
11. R. Etchenique and V. L. Brudny, *Langmuir*, **16**, 5064 (2000).
12. A. Bund, *J. Solid State Electrochem.*, **8**, 182 (2004).
13. H. Pagés, P. Topart, and D. Lemordant, *Electrochim. Acta*, **46**, 2137 (2001).
14. A. Bund and M. Schneider, *J. Electrochem. Soc.*, **149**, 331 (2002).
15. A. Arnau, Y. Jiménez, and R. Fernández, *345th Wilhelm und Else Heraeus Seminar: Acoustic Wave Based Sensors: Fundamentals, Concepts, New Applications (AWSW5)*, Apr 11–13 (2005), Bad Honnef, Germany.
16. L. Ochoa, Y. Jiménez, and A. Arnau, *XXVI Congreso Internacional de Ingeniería Eléctrica (Electro 2004)*, Chihuahua, Mexico, Oct 27–29, p. 139 (2004).
17. V. E. Granstaff and S. J. Martin, *J. Appl. Phys.*, **75**, 1319 (1994).
18. Y. Jiménez, M. Otero, and A. Arnau, in *Piezoelectric Transducers and Applications* 1st ed., A. Arnau, Editor, p. 255, Springer-Verlag, Berlin (2004).
19. L. Daikhin, E. Gileadi, G. Katz, V. Tsionsky, M. Urbakh, and D. Zagidulin, *Anal. Chem.*, **74**, 554 (2002).
20. R. Lucklum, D. Soares, and K. Kanazawa, in *Piezoelectric Transducers and Applications*, 1st ed., A. Arnau, Editor, p. 69, Springer-Verlag, Berlin, (2004).
21. S. J. Martin, V. E. Granstaff, and G. C. Frye, *Anal. Chem.*, **63**, 2272 (1991).
22. K. K. Kanazawa and J. G. Gordon, *Anal. Chem.*, **57**, 1770 (1985).
23. G. Sauerbrey, *Z. Phys.*, **155**, 206 (1959).
24. Y. Jiménez, Ph.D Thesis, Polytechnic University of Valencia, Valencia, Spain (2004).
25. Y. Jiménez, T. Sogorb, A. Arnau, M. Otero, and E. Calvo, *Proceedings of the Fourth Acoustic Wave Sensor Workshop AWSW-4*, Salbris, France (2003).
26. Y. Jiménez, R. Fernández, R. Torres, and A. Arnau, *IEEE Trans. Ultrason. Ferroelectr. Freq. Control*, In press.
27. R. Schumacher, G. Borges, and K. K. Kanazawa, *Surf. Sci.*, **163**, L621 (1985).
28. S. J. Martin, G. C. Frye, A. J. Ricco, and S. D. Senturia, *Anal. Chem.*, **65**, 2910 (1993).
29. M. Urbakh and L. Daikhin, *Langmuir*, **10**, 2836 (1994).
30. E. J. Calvo, E. S. Forzani, and M. Otero, *Anal. Chem.*, **74**, 3281 (2002).
31. *CRC Handbook of Chemistry, and Physics*, 80th ed., D. R. Lide, Editor, CRC Press, Boca Raton, FL (1999).
32. D. Johannsmann, J. Grunner, J. Wesser, K. Mathauer, G. Wegner, and W. Knoll, *Thin Solid Films*, **210**, 662 (1992).
33. A. R. Hillman, A. Jackson, and S. J. Martin, *Anal. Chem.*, **73**, 540 (2001).
34. A. Hammet and A. R. Hillman, *J. Electrochem. Soc.*, **135**, 2517 (1988).
35. L. M. Abrantes and J. P. Correia, *Electrochim. Acta*, **44**, 1901 (1999).
36. H. Randriamakazaka, V. Noel, and C. Chevrot, *J. Electroanal. Chem.*, **472**, 103 (1999).
37. L. Niu, C. Kvarnström, K. Fröberg, and A. Ivaska, *Synth. Met.*, **122**, 425 (2001).
38. I. Efimov, S. Winkels, and J. W. Schultze, *J. Electroanal. Chem.*, **499**, 169 (2001).
39. E. J. Calvo, C. Danilowitz, E. Forzani, A. Wolosiuk, and M. Otero, in *Biomolecular Films: Design, Function and Applications*, J. Rusling, Editor, Chap. 7, pp. 337–380, Marcel Dekker, New York (2003).
40. F. Höok, B. Kasemo, T. Nylander, C. Fant, K. Scott, and H. Elwing, *Anal. Chem.*, **73**, 5796 (2001).